Experimental and theoretical surface core-level shifts of aluminum (100) and (111)

Mikael Borg,[1] Martin Birgersson,[2] Maria Smedh,[1] Anders Mikkelsen,[1] David L. Adams,[3,*] Ralf Nyholm,[4] Carl-Olof Almbladh,[2] and Jesper N. Andersen[1]

[1]*Department of Synchrotron Radiation Research, Institute of Physics, Lund University, Box 118, S-221 00 Lund, Sweden*

[2]*Department of Solid State Theory, Institute of Physics, Lund University, Box 118, S-221 00 Lund, Sweden*

[3]*Institute of Physics and Astronomy, Aarhus University, DK-8000 Aarhus C, Denmark*

[4]*MAXLAB, Lund University, Box 118, S-221 00 Lund, Sweden*

(Received 14 May 2003; revised manuscript received 13 October 2003; published 30 June 2004)

The surface core-level shifts of Al(111) and Al(100) have been measured using high-resolution core-level photoemission spectroscopy and calculated using density functional theory (DFT). For Al(100), the 2*p* core-level shift of the first (second) layer was determined to be −75 meV (+20 meV) from experiment and −71 meV (+20 meV) from the DFT calculations. For Al(111), the corresponding values are −27 meV (0 meV) from experiment and −14 meV (−) from the DFT calculations. Core-level splittings caused by the low-symmetry crystal fields at the (111) and (100) surfaces have also been studied. These splittings turn out to be much smaller than previously reported provided proper care is taken of the influence of the core hole screening and of core–valence exchange beyond the DFT level. Finally, the experimental Al 2*p* line shape was found to contain structure caused by a sharp no-phonon line and a broad and weak phonon replica.

DOI: 10.1103/PhysRevB.69.235418 PACS number(s): 68.47.De, 79.60.Bm, 71.70.Ej

I. INTRODUCTION

The use of core-level binding energy shifts in high resolution core-level photoemission is a well established tool for studying clean and adsorbate covered surfaces. Due to large improvements of the achievable resolution it is today possible to resolve very small chemical shifts and/or to determine such shifts with unprecedented accuracy. Also these improvements allow for accurate studies of the core-level line shape. High resolution core-level photoemission experiments are being increasingly combined with full scale *ab initio* calculations of the core-level binding energy shifts. Taking full advantage of the high precision experimental results requires a high numerical accuracy of the core-level binding energy shift calculations and inclusion of a number of effects which influence the core-level spectra. In the present work we present very high resolution core-level photoemission spectra from two low index Al surfaces. We give a theoretical analysis of the experimental results including full *ab initio* calculations of the observed surface core-level binding energy shifts and the effects of the nonspherical potential experienced by a surface atom and briefly touch upon the influence of vibrational effects on the Al 2*p* core-level line shape.

Clean aluminum surfaces have been studied extensively, both experimentally, using photoemission spectroscopy[1–6] as well as photoemission partial yield measurements,[7] and theoretically using thermodynamical models, see e.g., Refs. 2 and 3, molecular orbital cluster based calculations[4] and by methods based on density-functional theory (DFT)[8–10] at various levels of sophistication. Actually, the Al(100) surface was among the first for which a surface core-level shift (SCLS) was determined experimentally[1] and in addition the first calculation[8] of a SCLS with full inclusion of final state effects was performed for this surface. For the Al(100) surface, the reported experimental values for the SCLS range from +310 meV[4] (+ sign indicates that the surface atoms have the larger core-level binding energy) to −120 meV,[7] however, a negative Al(100) SCLS with a magnitude slightly below 100 meV seems to be the accepted value today.[3,5] For the close-packed Al(111) surface no emission attributable to surface atoms has been identified and Nyholm *et al.*[3] estimated the SCLS of this surface to be smaller than 15 meV. On the theoretical side, values for Al(100) range from +630 meV[4] to −120 meV[9] whereas for Al(111) a value close to zero has been reported.[10] Furthermore, for Al(100), the good agreement between Feibelman's calculated[8] value of −97 meV and the more recent high resolution experimental values[3,5] has been suggested,[10] at least partly, to be a fortuitous effect of using the $Z+1$ approximation for describing the core ionized Al atom.

The reason for the large interest in the SCLS of Al surfaces lies in the simple electronic structure of Al. Al metal is often considered as a good approximation to the free electron gas making it an important model system. Furthermore the simple electronic structure makes high precision *ab initio* calculations less demanding in terms of computational resources, e.g., fewer plane waves are needed in the basis set than what is the case for transition metals. Also on the experimental side Al is an excellent material for high precision determinations of the SCLS. The binding energy of the Al 2*p* level is quite low and the level has large cross section making it easier to obtain good resolution at high count rates. Furthermore, the Al 2*p* level of Al metal turns out to be a very sharp level due to the relatively long lifetime of a 2*p* hole and, of equal importance, due to the weak coupling to phonons of such a 2*p* hole. In view of the fundamental importance of Al surfaces, the rather inconclusive state, experimentally and theoretically, concerning the SCLS therefore seems unsatisfying.

The paper is organized as follows. In Sec. II we describe our experimental setup, the theoretical background is summarized in Sec. III, Sec. IV gives our experimental results

and relate them to the present calculation and other theoretical results, and in Sec. V we give some concluding remarks.

II. EXPERIMENT

The experiments were performed at beam-line I311 at the MAX-II storage ring in Lund, Sweden.[11] The beam line is equipped with an SX-700 monochromator and a hemispherical Scienta SES 200 electron analyzer.

The crystals were cleaned by cycles of argon ion sputtering followed by annealing to about 450 °C. The surface contamination was monitored throughout the experiment by measuring C and O 1*s* spectra. Lateral surface ordering was checked using low energy electron diffraction (LEED). All measurements were performed at liquid nitrogen temperature in order to minimize peak broadening from phonons and electron–hole pair excitations, under ultrahigh vacuum conditions (below 10^{-10} Torr). The spectra were recorded at normal emission. To identify bulk and surface peaks, spectra were measured at different photon energies, ranging from 85 eV to 150 eV. Maximum surface sensitivity was found to be at about 95 eV. Total experimental resolutions were in the range 10–15 meV.

III. THEORETICAL BACKGROUND AND DFT CALCULATIONS

A. Total energy based calculations of core-level shifts

Core-level spectra in solids can usually be modeled as a sudden removal of an electron in a particular core shell. In this process, we can reach different final states where the core level is empty but where the valence electron system is in different excited states. The probabilities for reaching the different final states determine the core-level line shape. To the extent that lifetime effects can be left out, the core–electron spectrum has a well-defined threshold ϵ_c corresponding to complete relaxation of the valence electrons. Thus the core-level energy can be calculated as the difference in total energy of an unionized ground state with no core hole ($n_c=1$) and a final state with a core vacancy ($n_c=0$) and completely relaxed valence electrons, i.e., as $\epsilon_c = E(n_c=1) - E(n_c=0)$. The relaxed final state is, as far as the valence electrons are concerned, very similar to a ground state which is why this formally excited state is well described by a ground-state theory like DFT.[12,13]

The semi-infinite bulk plus surface is in a standard way described via use of (repeated) slabs separated by a vacuum layer of sufficient thickness for making the interslab interactions negligible. The isolated core hole in the final state is modeled by placing the ionized atom in a (lateral) supercell large enough that the interactions between the ionized atoms has a negligible influence on the core-level binding energy shifts. Core-level binding energies of atoms in various layers are then calculated as the difference in total energies of the slab without a core hole (initial state) and with a core hole (final state) from which the layer-dependent core-level shifts follow.

We have used both norm-conserving pseudopotentials combined with plane-wave (PW) basis sets and all-electron methods based on the linearized augmented plane-wave (LAPW) method.[14] In schemes based on norm-conserving pseudopotentials, Coulomb potentials and orbital eigenvalues are highly transferable. However, total energies probe the charge density and pseudopotentials in the core region where they have no direct physical meaning. As a result, total (pseudo-) energies may have larger transferability errors.[15–17] Our all-electron results allow us to estimate such errors, and with our choice of pseudopotential parameters (core radius, etc.) we find them to be small.

In our plane-wave calculations we used an implementation by Bockstedte *et al.*[18] and pseudopotential parametrization according to Hamann.[19] In the calculations for obtaining the pseudopotentials we used the Al ground-state configuration $2p^6 3s^2 3p$ as free-atom reference state. In order to model $2p$ core-excited Al states we chose the $2p^5 3s^2 3p^2$ configuration. In order to determine a suitable value for the pseudopotential radius r_c, we performed transferability tests where the difference in total energy between the Al pseudoatom and Al metal was evaluated as a function of r_c. In this way we minimize the transferability errors mentioned above. The r_c values were used for ground-state and core-excited ions. In the LAPW calculations we used the WIEN2k code by Blaha *et al.*[20] as well as a local implementation. An energy cutoff of up to 9.5 Ry was used and local orbitals of *s*, *p*, and *d* symmetry were added in order to minimize linearization errors.

The exchange–correlation functional was described by a generalized gradient approximation (GGA) by Perdew, Burke, and Ernzerhof,[21] except in our calculations of surface-induced core-level splittings where we used the local-density approximation (LDA). As reported earlier,[17] the GGA improves the geometrical parameters (lattice constant, surface relaxation, etc.), but with given geometrical parameters GGA and LDA give almost indistinguishable core-level shifts. Bulk calculations yielded an equilibrium lattice constant of 4.05 Å and a bulk modulus of 0.75 Mbar, in excellent agreement with the experimental values 4.05 Å and 0.77 Mbar.

The convergence with respect to slab thickness will be discussed in the following section, here we just mention that we used up to 13 layers for ground-state systems and up to nine layers for core-excited systems. The thickness of the vacuum layer separating slabs was also varied and increased until the level shifts were converged within a few meV. In order to check for interaction between excited sites of the final state slabs we varied the size of the lateral unit cell. For the (100) surface, $c(2\times2)$, (2×2), and $c(4\times4)$ lateral unit cells were studied whereas for the (111) surface, (2×2) and (3×3) cells were considered. Based on these tests, we judge that the SCLS is numerically converged to better than ±5 meV by use of 2×2 unit cells and 45, 105 irreducible *k*-points 2×2 Brillouin (2D) zones of the Al(100) and Al(111) slabs, respectively.

B. Geometrical parameters

The interlayer spacings of the outermost surface layers turn out to have significant relative, albeit not absolute, influence on the calculated SCLS. These interlayer spacings

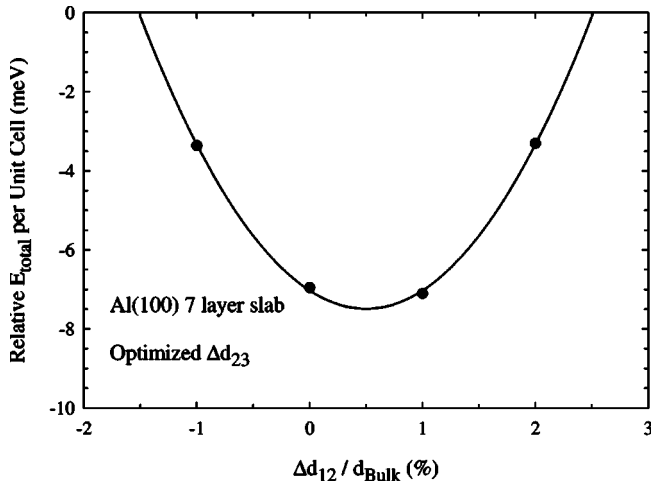

FIG. 1. The variation of the total energy of a seven-layer Al(100) slab with the relaxation Δd_{12} of the first interlayer spacing. For each value of Δd_{12}, an optimization has been performed of the second interlayer spacing d_{23}.

are determined by minimizing the total energy with respect to them. However, close to the minimum the total energy depends only weakly on the spacings. This presents severe demands on the computational accuracy of the minimization procedure and, in our opinion, the uncertainty in the SCLS induced by the resulting uncertainty in the interlayer spacings is actually larger than that induced by numerical inaccuracies of the calculations. In Fig. 1 we show as an example how the total energy per unit cell of the Al(100) slab varies with the deviation Δd_{12} of the first interlayer spacing from the bulk value.[38] A 1% change of Δd_{12} from the optimum value is seen to induce a change of the total energy of less than 2 meV. Similar results are obtained for Al(111). In view of this weak variation we believe that the interlayer relaxations cannot be determined to better than a few percent from DFT. The DFT optimum values of the interlayer spacings are given in Table I. As seen from Table I, the agreement with experimental determinations[22,23] is reasonable for both surfaces. The influence of these geometrical uncertainties is illustrated in Table II which shows the calculated first and second layer core-level shifts for several d_{12} and d_{23} combinations. As seen, small changes of the interlayer spacings compatible with experiment[22,23] lead to changes of the core-level shifts which, although not large on an absolute scale, are significant relative to the shifts themselves. The aforementioned uncertainty of the interlayer distances thus translates into a significant relative (but small absolute) variation of the calculated core-level binding energy shifts. In passing we note that, as discussed previously,[17] the strong interlayer spacing dependence of the binding energy is due to the final state atom not being in geometrical equilibrium after the vertical core ionization. Away from equilibrium, the total energy has a steeper dependence on the geometrical parameters like, e.g., the interlayer distances (see Fig. 1). Therefore geometrical changes around the equilibrium which only create a small total energy change for the initial state may result in a significantly larger change for the final state total energy, and thereby cause a large change of the core-level binding energy.

TABLE I. Surface relaxations relative to the bulk interlayer distance.

	100		111	
	Expt.[a]	Theor.	Expt.[b]	Theor.
Δd_{12}	+2.0%	+0.5%	+1.4%	+2.0%
Δd_{23}	+1.2%	−0.3%	0.0%	

[a]From Ref. 22.
[b]From Ref. 23.

TABLE II. Calculated core-level shifts for the first (SCLS) and second (L2CLS) layer of Al(100) and Al(111) for different first- (Δd_{12}) and second- (Δd_{23}) interlayer relaxations. LAPW-based shifts are decomposed in initial-state (Δ_i) and relaxation (Δ_r) components. The shifts are given relative to the middle layer of the respective slabs. Energies in meV.

	Δd_{12}	Δd_{23}	Method	SCLS	Δ_i	Δ_r	L2CLS
111	0%	0%	[a]	−36			
111	1.4%	0%	[a]	−14			
100	0%	0%	[a]	−101			−2
100	2%	1.4%	[a]	−86			7
100	2%	1.4%	[b]	−71			20
100	2%	1.4%	[c]	−96	6	−102	11

[a]PW, seven-layer slab.
[b]PW, nine-layer slab.
[c]LAPW, seven-layer slab.

Second, the determination of the reference bulk binding energy with a precision of a few meV turns out not to be straightforward when using the slab-based method. If one uses a separate bulk supercell, one is forced to use different k point grids for different supercells and cannot rely on cancellation of errors in the k-space integration when comparing slab and bulk total energies. If one instead uses the middle layer of the vacuum-separated slabs as the reference, one finds that it is not quite stable with regard to slab thickness. The underlying reason for this is that Friedel oscillations from the two surfaces of the slab have a slow asymptotic fall-off. In the case of symmetric slabs, these Fermi-surface driven oscillations interfere and will be commensurate with a wavelength somewhat longer than the Fermi wavelength. As a result, the Hartree potential of the inner layers of the slab shows variations of the order 10–20 meV causing the core-level binding energies to fluctuate even for the inner layers of the slab. We illustrate this effect in Fig. 2 which shows the layer dependent (initial) state Al $2p_{3/2}$ eigenvalues obtained from LAPW calculations for several Al(100) slab thicknesses. We notice that the relative shifts between the outermost layers converge more rapidly than do the shifts of the middle layers. Thus, the boundary conditions emerging from the surface seem to make the orbitals more stiff near the surface than near the center. We have found that the orbitals of jellium slabs also show this general behavior with regard to slab thickness. In our case, the Friedel fluctuations in the

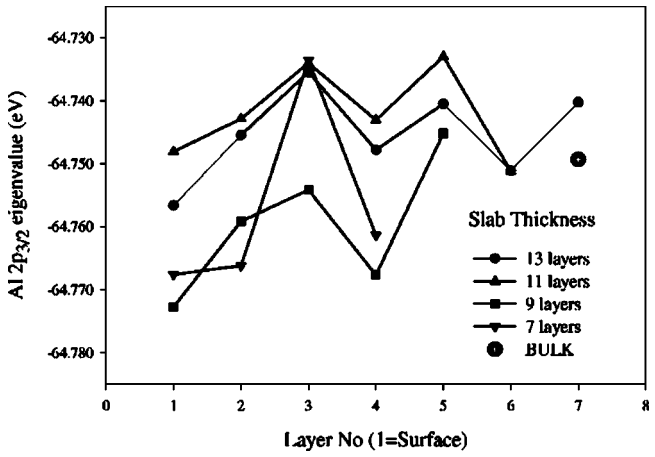

FIG. 2. The Al $2p_{3/2}$ eigenvalue, relative to the Fermi level, at different layers and for different slab thicknesses from LAPW ground-state calculations.

middle layers amount to about 10 meV in an 13-layer slab.

We have performed a similar analysis also for the Al(111) surface. In this case the Friedel oscillations have a smaller amplitude, and we find that the middle layer from a seven-layer slab should furnish a bulk reference accurate to 5 meV or better. One explanation why the Al(111) surface converge better with respect to slab thickness is of course the longer interlayer spacing for closed-packed surfaces. Another reason could be that standing-wave patterns emerge more easily along the (100) direction. In the case of the (100) surface, the interlayer separation is almost commensurate with half a Fermi wavelength, and this seems to favor an alternating behavior of the Hartree potential.

We have also studied the behavior of the relaxation energy and obtained indication that this part of the core shift exhibits smaller oscillations. This is in agreement with the general expectation that the 0-dimensional perturbation from a core hole should be weaker than a two-dimensional perturbation from a surface.

Using the experimentally determined interlayer distances and a nine-layer slab we obtain shifts relative to the bulk emission of −71 meV (minus sign indicates a shift toward lower binding energy) and +20 meV, respectively, for the first and second layer SCLS of the Al(100) surface. For the Al(111) surface we obtain a SCLS of −14 meV from seven-layer slabs. These estimates are based on PW results and the bulk reference has been approximated by the middle layer of the slab. We notice in Table II that the PW and LAPW results are consistent within about 10 meV. Finally, it is noticeable that the binding energy shifts between the first and second layers show much better agreement between the seven- and nine-layer slabs than the individual shifts. The larger change of the individual shifts can be rationalized as due to the use of the bulk level as reference energy and the aforementioned difficulties caused by variations in the Hartree potential for the middle layer of a finite slab.

When comparing with other works, we first want to point out that a comparison to experimental data as described in a later paragraph shows a good agreement between experiment and theory for the surface related core-level shifts of Al(111) and Al(100). Second, the agreement with an earlier calculation of the SCLS by Feibelman[8] for Al(100) is also good. This earlier calculation used a 0.4% inwards relaxation of the surface layer ($\Delta d_{12}=-0.4\%$) as opposed to the currently used outwards relaxation of 2%. However, if we use the same geometry as Feibelman we obtain a shift of about −103 meV for a seven-layer slab, to be compared to Feibelman's value of −96 meV. Aldén *et al.*,[10] on the other hand, obtained an almost vanishing SCLS for Al(100) and furthermore argued that the excellent agreement between Feibelman's calculated value and experimental results was partly a side effect of the $Z+1$ approximation used in the calculation. In order to test this we have calculated the SCLS of Al(100) for the experimental geometry by use of the $Z+1$ approximation. We obtain a $Z+1$ value of −120 meV demonstrating that the $Z+1$ approximation results in a roughly 30% increase of the calculated SCLS. Thus the good agreement obtained by Feibelman cannot be solely ascribed to his use of the $Z+1$ approximation. It should also be noticed that the value of the Al(100) SCLS calculated by Aldén *et al.* disagrees with both experiment as well as with the current calculations. Even though we have not investigated this point in detail, we would still believe the discrepancy to be a result of the use of the atomic sphere approximation (ASA) by these authors. The SCLS of these surfaces are of such small magnitude that errors introduced by approximations like ASA may become very significant.

Finally, it may be noted that the SCLS perhaps somewhat counter-intuitively shows an increase when d_{12} is decreased and the surface layer is placed in a more bulklike environment. As the total energy of the initial state slab only depends weakly on the interlayer spacing in the vicinity of the minimum, the variation of the SCLS may to a good approximation be ascribed to the variation of the total energy of the final state slab with interlayer spacing. Therefore the increase of the SCLS with decreasing d_{12} simply signifies that the total energy of the final state slab decreases with decreasing d_{12} which in turn shows that the minimum of the total energy for the final state slab occurs for a smaller d_{12} value than found in the initial state slab.

C. Line shapes in core-level photoemission

Several effects of electronic origin contribute to the fundamental line shape of a core-level photoemission peak from a metallic system; the finite lifetime of the core hole, the shake-up of electron-hole pairs during the photoemission process, and broadening originating from thermally excited valence electrons.

In theoretical modeling, the effects of finite core-hole lifetime is usually added as an afterthought by convoluting by a Lorentzian broadening. Commonly, the so-called Doniach–Šunjić[24] line shape is used as model function for the components in core-level photoemission from metallic systems. This line shape contains a Lorentzian distribution originating from the finite lifetime, and a Mahan–Nozières–de Dominicis[25–27] (MND) asymmetry index α, which accounts for creation of particle-hole pairs during the photoemission process. In the case of the Al $2p$, the valence

electrons are involved both in the core-hole relaxation and in the core-hole annihilation, and some interference might be expected. For long lifetimes, however, the only important interference is believed to be a renormalization of the decay rate which should be determined by the fully relaxed hole state.[28] Detailed calculations have been made by Almbladh *et al.*[29] which demonstrate the importance of core-hole relaxation on the level widths.

The derivation of the Doniach–Šunjić line shape assumes that the temperature T of the electron gas is 0 K. At finite temperatures, thermally excited particle-hole pairs also couple to the core hole via the MND mechanism and broaden the core line. In many cases this broadening is adequately described by its second-order moment and can be taken as Gaussian with a full width at half-maximum (FWHM) of $2.35\pi kT\sqrt{\alpha/3}$.[30] For aluminum at 100 K this amounts to about 8 meV which, even though small on an absolute scale, is significant when compared to lifetime widths (FWHM) in the range of 20–30 meV as determined experimentally for Al $2p_{3/2}$.

The core-level line shape is also affected by disorder and the fact that the nuclei are vibrating. Disorder broadening originates from core holes at different positions with different local environment and thus slightly different binding energies. Disorder broadening would be absent in the bulk of a perfect crystalline solid but is usually present at surfaces owing to steps and other imperfections.

The broadening from lattice vibrations originates from the fact that core-level energy depends on the instantaneous positions of the nuclei. This dependence gives a coupling between the core level and the phonons. In a semiclassical picture this leads to a Gaussian broadening which reflects the magnitude of the lattice displacements and the core-hole–lattice coupling. In a quantum-mechanical description, the phonon broadening is a shake-up phenomenon, with a no-phonon line corresponding to full lattice relaxation and satellites corresponding to phonon shake-up. When the number of shake-up phonons $\overline{n}$ is large, the quantum and classical descriptions become equivalent. In the case of Al, the phonon broadening was calculated long ago by Hedin and Rosengren,[31] who found a very small broadening with $\overline{n}\simeq 0.6$. In this limit the phonon broadening is not at all Gaussian but instead consists of a no-phonon line and a one-phonon satellite with a relative strength of the order $\overline{n}$. In our analysis we therefore model the vibrational effects by a main line plus a weak phonon replica with a width of the order of the phonon bandwidth.

D. Crystal field splitting

At surfaces the ion cores experience low-symmetry crystal fields which in principle may split the core level in subcomponents. At the (100) and (111) surfaces, symmetry allows for crystal fields involving $l=1$ and $l=2$ spherical harmonics. In the case of $2p$ core holes, the $l=2$ components couple in first order and the $l=1$ components in second order and split $j=3/2$ hole states in two components corresponding to magnetic sublevels $\pm 3/2$ and $\pm 1/2$.

The $m_j=3/2-1/2$ splitting at the Al(100) surface has been estimated earlier by Wimmer *et al.*,[9] who obtained a value of 40 meV. However, our experiments indicate a substantially smaller value, and therefore we have reinvestigated the matters. There are two important ingredients which we believe have not properly been accounted for earlier. First, the crystal fields give no splitting of the initial ground state total energy ($E^0(N)$) as this state has filled core levels ($^1S_0$ symmetry). The final state, however, has only fractional occupancy of the core level, thus allowing for an explicit m_j dependence of the total energy $E^*(N-1,m_j)$. As $E_B=E^*(N-1,m_j)-E^0(N)$, it is evident that the splitting is determined by the final-state potential with a core-hole impurity rather than the ground-state potential. Second, the core-level splitting is probing the internal structure of the core level [the value of the magnetic (m_j) quantum number], and we find that ground-state DFT is a poor approximation to the crystal field part of the m_j dependence of the core-valence exchange interaction. The core-valence exchange amounts to about 30% of the Coulomb part in a DFT description and is of opposite sign. If we instead use the full core-valence exchange operator, we obtain much larger values which, in the case of Al, almost balance the direct Coulomb part.

We first describe the DFT mean-field calculations and come back to the exchange corrections at the end of this section. In order to obtain reliable potentials in the core region an all-electron method is preferred. We used the LAPW method as described above. The shifts from V_{20} are readily obtained as $\Delta_{jm}^{(20)}=Q_2\langle\mathcal{Y}_{1jm}|Y_{20}|\mathcal{Y}_{1jm}\rangle$, where Q_2 is a radial integral, Y_{lm} a spherical harmonic, and $\mathcal{Y}_{ljm}$ a spin spherical harmonic. The Gaunt coefficient $\langle\mathcal{Y}_{ljm}|Y_{20}|\mathcal{Y}_{ljm}\rangle$ has the values $\pm 1/\sqrt{20\pi}$ for $j=3/2$ and $m=3/2,1/2$ and are the same for the two allowed values of l which arise from the large and small components of the core orbital. V_{20} does not shift the $j=1/2$ core level. The shifts were calculated using both a fully relativistic as well as a nonrelativistic core orbital. The detailed results for the (100) surface are summarized in Table III. The relativistic and nonrelativistic results are almost indistinguishable. Shifts induced by the ground-state potential are also given in Table III and are found to agree very well with the earlier results by Wimmer *et al.*[9] As seen in Table III, core-hole screening reduces $\Delta_{jm}^{(20)}$ by about a factor of 4.

The second-order shifts from V_{10} were obtained using the Schrödinger rather than the Dirac equation, which should be adequate owing to the smallness of the relativistic corrections. The shifts can be expressed as $\langle\psi_0|V_{10}|\psi_1\rangle$ in terms of the unperturbed (ψ_0) and perturbed (ψ_1) parts of the core orbital. The perturbed part ψ_1 is obtained from a Schrödinger equation with the perturbation in a source term. Separating angular and radial parts we write $V_{10}(\mathbf{r})=v_{10}(r)Y_{10}(\hat{r})$, $\psi_0(\mathbf{r})=P_{2pj}(r)/r\ \mathcal{Y}_{1jm}(\hat{r})$, and $\psi_1(\mathbf{r})=(P_{lj'}(r)/r)\ \mathcal{Y}_{lj'm}(\hat{r})\times\langle\mathcal{Y}_{lj'm}\,|Y_{10}|\mathcal{Y}_{1jm}\rangle$. The perturbed radial parts of the core orbital follow from

$$[\epsilon_{2pj}-h_{lj'}^{(0)}]P_{lj'}(r)=v_{10}(r)P_{2pj}(r), \tag{1}$$

where ϵ_{2pj} is the unperturbed energy eigenvalue and $h_{lj'}^{(0)}$ the radial Hamiltonian for angular momenta lj'. The second-order shifts are then obtained from

TABLE III. Crystal field splitting (meV) of the $2p$ level at the Al(100) surface from DFT for ground state (gs) and core excited (excited) nonspherical (NS) potentials, using fully relativistic (rel) as well as nonrelativistic (nr) core orbitals.

NS potential		$j=\frac{1}{2}$	$j=\frac{3}{2}$ $m=\frac{1}{2}$	$j=\frac{3}{2}$ $m=\frac{3}{2}$	$j=\frac{3}{2}$	Average
(a) V_{20} nr	Excited	0	5.789	−5.789		0
(b) V_{20} rel	Excited	0	5.788	−5.788		0
(c) V_{20} rel	gs	0	19.1	−19.1		0
(d) V_{10} nr	Excited	1.5	3.9	−0.8		1.5
(e) V_{10} nr	gs	−0.005	−0.007	−0.003		−0.005
$V_{10}+V_{20}$	Excited	1.5	9.7	−6.6		1.5
$V_{10}+V_{20}$	gs	−0.005	19.1	−19.1		−0.005

$$\Delta_{jm}^{(10)} = \sum_{lj'} \langle P_{2pj}|v_{10}|P_{lj'}\rangle|\langle \mathcal{Y}_{lj'm}|Y_{10}|\mathcal{Y}_{1jm}\rangle|^2. \qquad (2)$$

The relevant Gaunt coefficients $\langle \mathcal{Y}_{lj'm}|Y_{10}|\mathcal{Y}_{1jm}\rangle$ are given in Table IV. By parity, l is 0 or 2, and the angular momentum j' for the perturbed part is limited by the usual angular momentum rules, $|j-1|\leqslant j'\leqslant j+1$ and $|l-1/2|\leqslant j'\leqslant l+1/2$.

The spin–orbit coupling is very weak in comparison with the total effective potential, and as a consequence the j dependence of the radial wave functions can to a very good approximation be neglected. The splitting originates almost exclusively from the Gaunt coefficient in Eq. (2) which weights the s and d waves differently for the different sublevels jm. The d wave contributes very small shifts downward, and the s wave a larger shift upward. In Table IV we see that the s wave only couples to the sublevels with $m=\pm 1/2$, which consequently are shifted up, and the shift of the levels with $j=3/2$ are shifted about twice as much as the $j=1/2$ levels. The sublevels with $m=\pm 3/2$ only couple to the d wave and exhibit a small negative shift. As seen from Table III, V_{10} gives rise to a small shift of both j levels and a splitting of the $j=3/2$ level. The V_{10} induced splitting is only about 20% of that induced by V_{20}. However, as shown below a more correct treatment of exchange and correlation reduces the V_{20} contribution to a level where V_{10} becomes responsible for a significant part of the total splitting.

We now turn to the exchange contribution to the core-level shifts. In Table V we have separated out the exchange–correlation part as obtained from ground-state DFT. It is seen that in DFT this contributes about 30% to the shifts and is of opposite sign as the Coulomb part. The details of the core-valence exchange depends explicitly on the magnetic sublevel indices of core and valence electrons. It is not clear that such an explicit state dependence is well described by a ground-state DFT potential. If we use the full core-valence exchange operator, the shifts for uncoupled $l_c m_c s_c$ core orbitals depend on m_c but not on spin. The origin of the m_c dependence is the lower symmetry of the valence-electron wave function at the surface than in the bulk. It is convenient to split the exchange potential into an average over magnetic sublevels and a remainder. The sublevel dependent remainder can be written[32]

$$\langle l_c m_c|\Sigma_x^{(1)}|l_c m_c\rangle = \sum_{l''m''lm} n_{lm} Q_{l''}(l,l) B_{mm''m_c}^{ll''l_c}, \qquad (3)$$

where $B_{mm''m_c}^{ll''l_c}$ contains Wigner $3j$ symbols,[33]

$$B_{mm''m_c}^{ll''l_c} = \begin{pmatrix} l & l'' & l_c \\ -m & m'' & m_c \end{pmatrix}\begin{pmatrix} l_c & l'' & l \\ -m_c & -m'' & m \end{pmatrix} - \frac{1}{(2l+1)(2l_c+1)} \qquad (4)$$

and where $Q_{l''}$ is given by

$$Q_{l''}(k,k') = (2l+1)(2l_c+1)\begin{pmatrix} l & l_c & l'' \\ 0 & 0 & 0 \end{pmatrix}^2 \times R_{l''}(vl,c,c,vl) \qquad (5)$$

in terms of $3j$ symbols and radial core-valence exchange integrals $R_{l''}(vl,c,c,vl)$. In the calculations we approximated the radial valence-electron density matrix of l symmetry by an effective orbital $\phi_{lv}(r)$ normalized to one in the muffin-tin sphere, $\gamma_{lm}(r,r')=n_{lm}\phi_{lv}(r)\phi_{lv}(r')$ (n_{lm} is the number of valence electrons of lm symmetry in the core-hole sphere). Having obtained the splits in a $l_c m_c$ representation, the split-

TABLE IV. Gaunt coefficients $|\langle \mathcal{Y}_{lj'm}|Y_{10}|\mathcal{Y}_{1jm}\rangle|^2$.

$lj'\backslash jm$	$\frac{1}{2}\ \frac{1}{2}$	$\frac{3}{2}\ \frac{1}{2}$	$\frac{3}{2}\ \frac{3}{2}$
$s_{\frac{1}{2}}$	$1/12\pi$	$1/6\pi$	0
$d_{\frac{3}{2}}$	$1/6\pi$	$1/300\pi$	$3/100\pi$
$d_{\frac{5}{2}}$	0	$9/50\pi$	$3/25\pi$

TABLE V. Contribution to the crystal field splittings for the $2p_{3/2}$ level of surface atoms on Al(100) and Al(111) from the Coulomb potential V_C, the DFT v_{xc} potential, and the full core–valence exchange (Σ_x). Energies in meV.

Surface	V_C	v_{xc}	Σ_x	$V_C+\Sigma_x$
Al(100)	20.2	−3.9	−16.1	4.1
Al(111)	25.6	−5.2	−22.8	2.8

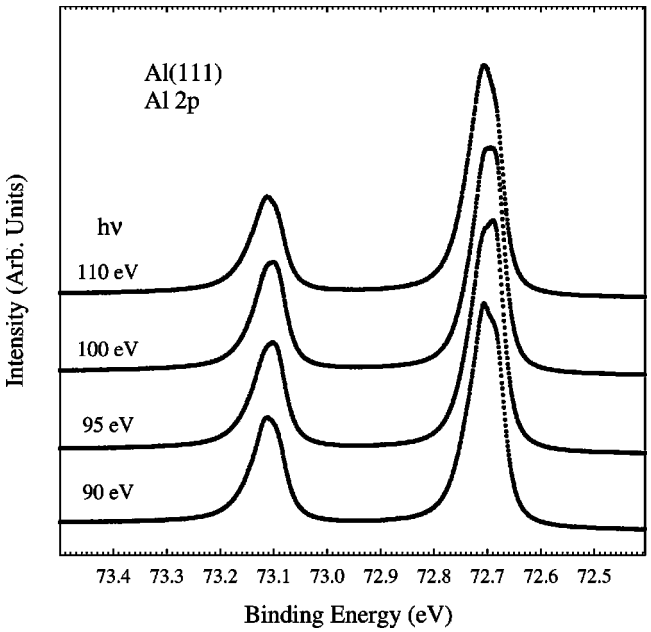

FIG. 3. Al 2*p* spectra from Al(111) measured at the indicated photon energies. Measured at 100 K and normal emission.

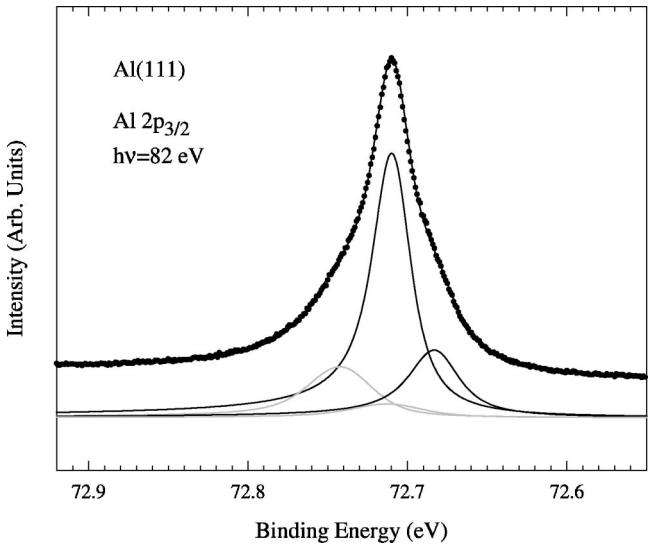

FIG. 4. Bulk sensitive Al $2p_{3/2}$ spectrum from Al(111) excited at a photon energy of 82 eV. A decomposition into bulk (higher binding energy) and surface (lower binding energy) components is included. Each of these components consists of a no-phonon line (black line) and a phonon replica (grey line). The resulting fit is included (black line).

tings for spin–orbit coupled core levels are obtained by transformation to $j_c m_c$ core orbitals,

$$\langle j_c m_c|\Sigma_x^{(1)}|j_c m_c\rangle = \sum_{m_c s} |\langle 1/2, l_c; s, m_c - s|j_c m_c\rangle|^2 \times \langle l_c m_c|\Sigma_x^{(1)}|l_c m_c\rangle. \quad (6)$$

The results for the Al(100) and Al(111) surfaces are given in Table V. The pure Coulomb contributions to the $3/2-1/2$ splits are about the same for the two surfaces. [In the case of Al(111), the $l=1$ crystal field gives a negligible contribution.] The DFT potential counteracts the Coulomb part and gives a negative contribution about 20% of the direct part. The full core-valence exchange gives a substantially larger contribution, and when we correct we obtain very small total shifts. Finally, we would like to stress that it is not the average core-valence exchange which is grossly misrepresented by DFT, it is just the angle-dependent crystal field part.

IV. EXPERIMENTAL RESULTS AND ANALYSIS

Figure 3 shows Al 2*p* spectra from the Al(111) surface measured at different photon energies. These raw data directly show that both spin–orbit components contain two components which can be ascribed to emission from bulk and surface atoms, respectively. From the variation in relative intensity of the two components as the photon energy and thereby the escape depth is changed, the component at lower binding energy can be identified as the surface component, i.e., the SCLS of the Al(111) surface is negative. By simply reading off the peak positions in the raw data, the magnitude of the Al(111) SCLS may be estimated to between 20 and 30 meV. In order to improve the accuracy of this estimate, we have performed numerical decompositions of the Al 2*p* spectra using the FITXPS package.[34] Initially we used two Doniach–Šunjić components in order to simulate bulk and surface emission. This resulted in a SCLS of around −27 meV, however, the quality of the obtained fits were not satisfactory. A major reason for the failure is illustrated in Fig. 4 which shows an Al 2*p* spectrum measured at a photon energy of 82 eV, i.e., under bulk sensitive conditions. Due to the bulk sensitivity, the surface peak is visible only as a weak shoulder on the low binding energy side of the bulk peak thereby minimizing the influence of any surface related features. As seen from Fig. 4, the bulk peak exhibits a double structure with one very sharp component and a broader emission feature at slightly higher binding energy. This is exactly the shape expected for a case with only weak coupling to the phonons[31] as described in Sec. III C; a dominating no-phonon line and a weak structure at higher binding energy due to phonon losses (we neglect the phonon gain possibility at 100 K). In Fig. 4 we have used Doniach–Šunjić line shapes for both the no-phonon line and the phonon loss feature. The phonon induced structure, which has an intensity relative to the no-phonon line of about 0.4 and an approximately 30 meV higher binding energy, is significantly broader than the no-phonon line (total FWHM 50 meV and 30 meV, respectively, for the $2p_{3/2}$ spin–orbit component) and is furthermore almost Gaussian in shape. Introducing a similar double-peak line shape for the bulk and surface components in spectra measured under surface sensitive conditions clearly improves the quality of the fits (see Fig. 5), however, the Al(111) SCLS remains unchanged at a value of -27 ± 3 meV. This may be compared to our theoretical values of −14 meV and −36 meV using the experimental and bulk termination, respectively. Furthermore, from our tests with different methods (PW, LAPW) and different numerical parameters (basis set size, *k* points, etc.) we expect an overall accuracy of about 10 meV, and the difference between

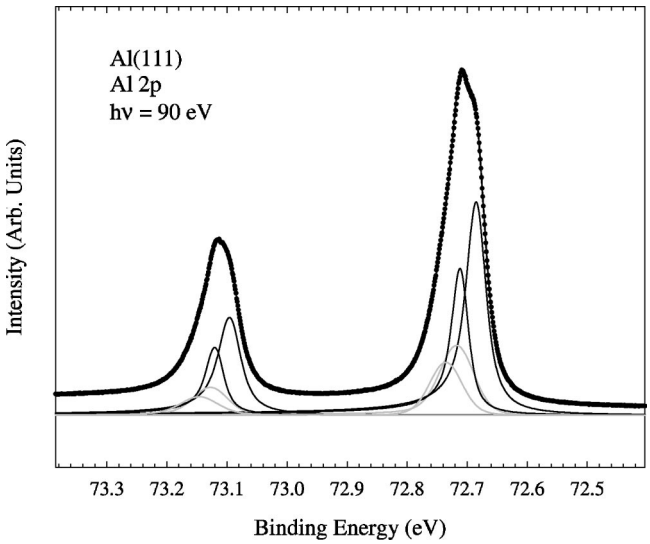

FIG. 5. Al $2p$ spectrum from Al(111) at a photon energy of 90 eV. A decomposition into surface (lower binding energy) and bulk (higher binding energy) components is included. Each of these components consists of a no-phonon line (black line) and a phonon replica (gray line). The resulting fit is included (black line).

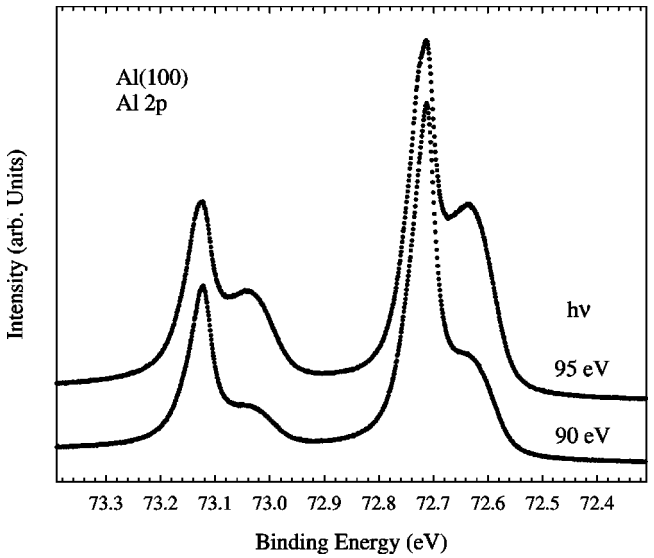

FIG. 6. Al $2p$ spectra from Al(100) measured at the indicated photon energies. Measured at 100 K and normal emission.

theory and experiment is of the same order as the estimated accuracy.

The Doniach–Šunjić line shape parameters of the $2p_{3/2}$ spin–orbit component obtained for the no-phonon lines of the bulk and surface emission are given in Table VI. Concerning these line shape parameters we note that precise determination of α is hampered by the existence of the phonon loss peak on the high energy side of the components, however, use of α values above 0.1 consistently results in poor decompositions. Concerning the widths we note that the uncertainties of the Lorentzian and Gaussian widths are strongly coupled; a reduction of say the Gaussian has to be compensated by a corresponding increase of the Lorentzian.

TABLE VI. Line shape parameters for the $2p_{3/2}$ component for Al(111) and Al(100). Γ_L and Γ_G are Lorentzian and Gaussian FWHM widths, and ΔE are binding energy shifts relative to the bulk peak. Energies in meV.

	Γ_L	Γ_G	α	ΔE
111				
Bulk	23±5	16±5	0.07±0.03	
Surface	23±5	23±5	0.07±0.03	−27±3
100				
Bulk	23±5	14±5	0.07±0.03	
Second layer	23±5	14±5	0.07±0.03	+18±2
Surface	23±5	55±10	0.07±0.03	−75±5[a]

[a]The value is the average for two crystal field split components corrected for the phonon structure. The value of −95 meV in Ref. 35 refers to the shift between no-phonon lines. For this we here obtain −96 meV.

The uncertainty of the total width is quite small. The surface component is found to be slightly broader than the bulk peak which at least partly is due to that we have neglected the crystal field split and only used one surface component. The calculated crystal field splitting is only 3 meV which is easily absorbed into a slightly larger width of the surface component. Additionally, disorder broadening is expected to be more pronounced for the surface than for the bulk peak as surface related disorder, e.g., steps, is more likely than bulk disorder. We also note that it is not possible to decompose the Al(111) spectra if the crystal field splitting of about 25 meV calculated without full inclusion of exchange and correlation is used for the surface component.

The determined lifetime width of around 23 meV is in excellent agreement with a previous calculation for the Al $2p$ level by Almbladh, Morales, and Grossmann[29] who calculated a value of 22 meV using orbitals relaxed in the presence of the core hole when calculating the decay rate. If the effects of the core hole are not included, a value of 11 meV is obtained which seems incompatible with the experimental data.

The strength of the phonon loss component is not easy to determine for the surface peak as it energetically coincides with the no-phonon bulk component. We are therefore not able to deduce any difference in phonon coupling for bulk and surface core ionization in the Al(111) case. Finally, the line shape parameters for the $2p_{1/2}$ components are identical to those of the $2p_{3/2}$ except for the Lorentzian width. This width is found to be about 10–15% larger for the $2p_{1/2}$ level reflecting that the deeper $2p_{1/2}$ level can decay into a $2p_{3/2}$ hole and an excited valence electron via the core-valence exchange interaction. The magnitude of this increase of the width furthermore shows an excellent quantitative agreement with recent theoretical calculations.[32]

Figure 6 shows two Al $2p$ spectra from the Al(100) surface measured at photon energies of 90 and 95 eV, respectively. Comparison of the surface sensitive 95 eV spectrum to the more bulk sensitive 90 eV spectrum first demonstrates,

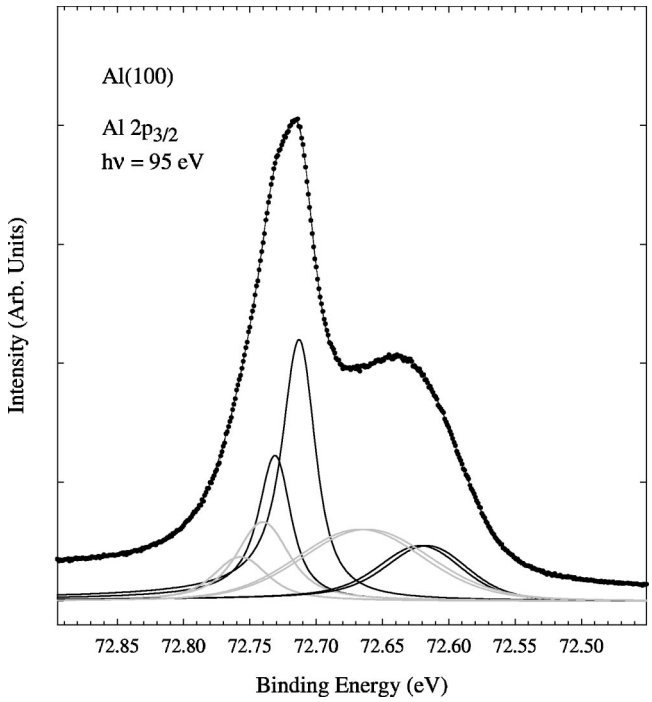

FIG. 7. Al $2p_{3/2}$ spectrum from Al(100) at $h\nu$=95 eV. A decomposition into second layer (higher binding energy), bulk (middle binding energy), and two crystal field split surface (lower binding energy) components is included. Each of these components consists of a no-phonon line (black line) and a phonon replica (gray line). The resulting fit is included (black line).

as expected,[1–6] a surface shifted component at lower binding energy relative to the bulk component. Simply reading off the peak positions of the 95 eV spectrum results in an Al(100) SCLS of around −80 meV, i.e., slightly smaller than previously reported. Second, the comparison also shows that a component at slightly higher binding energy than the bulk peak is seen under surface sensitive conditions. From the 95 eV spectrum, the binding energy of this component is estimated to be about 20 meV higher than that of the bulk peak. From the intensity behavior with photon energy, the obvious interpretation of this +20 meV component is to assign it to emission from the second Al layer. Such an assignment is furthermore in excellent agreement with the values calculated for the second layer shift of Al(100). As for the Al(111) case we have refined these estimates of the surface related core-level shifts by decomposing the spectra. For the bulk and the second layer component we use the same line shape as for the bulk peak of the Al(111) spectra including the phonon related structure. As seen from Fig. 7 use of this line shape results in excellent decompositions of the high energy part of the spectrum. For the surface peak we explicitly include the crystal field splitting of the $2p_{3/2}$ spin–orbit component. However, even if this crystal field splitting is allowed to deviate considerably from the calculated value of 4 meV, it is not possible to obtain satisfactory decompositions of the surface emission if a line shape similar to the surface or bulk line shape from Al(111) is used. In order to obtain an acceptable decomposition of the surface emission, it turns out to be necessary to use a stronger coupling to the phonons at the surface and also to increase the width of the no-phonon line. As seen from Fig. 7, these modifications of the surface emission line shape result in excellent decompositions also of the surface related emission. The shift between the no-phonon bulk and surface components is found to be about −96 meV. This shift, however, refers to final states which are fully relaxed geometrically whereas the calculated SCLS refers to vertical transitions, i.e., the same geometry in the initial and final states. Thus the −96 meV cannot be directly compared to the calculated SCLS. However, the vertical excitation energy can,[37] to linear order in the phonon coupling, be extracted from the experimental spectrum by performing a Franck–Condon analysis, i.e., by taking the intensity weighted average over the vibrational envelope. The parameters needed for such an analysis are given in Table VII. For the Al(111) case with similar vibrational envelopes for bulk and surface emission such an analysis of course yields the same result as obtained directly from the no-phonon lines. For Al(100), however, the stronger vibrational excitations for the surface peak will make the vertical SCLS smaller than that between the no-phonon lines. Performing the intensity weighted averaging we obtain an experimental value of −75 meV for the SCLS of Al(100) in excellent agreement with the range of theoretical values given in Table II. It is also gratifying to note that this experimental value is close to the −80 meV obtained from simple inspection of the data. We also note that the experimental value is quite robust when it comes to changes in the strength of the phonon induced structure as changes induced by variations of this strength is counteracted by changes of the no-phonon line binding energy required to maintain a good decomposition.

We now turn to a short discussion of the differences in bulk and surface line shapes on Al(100). However, before going into this we will note that the use of a Doniach–Šunjić component for describing the phonon induced structure is only an approximation. In particular for the surface emission where excitation of phonons is strong this approximation may be a major reason for some of the deviations from the bulk values. Concerning a more correct description of the

TABLE VII. Summary of phonon structure parameters for the various Al $2p_{3/2}$ components of Al(111) and Al(100). ΔE_{ph} is the energy shift between the no-phonon line and the phonon induced structure, I_{ph}/I_0 is the intensity of the phonon induced structure relative to that of the no-phonon line, FWHM is the full width at half maximum of the phonon induced structure. All energies in meV.

Component		ΔE_{ph}	I_{ph}/I_0	FWHM	
				No-phonon	Phonon
111	Bulk	30	0.4	30	50
	Surface	30	0.4	30	50
100	Bulk	30	0.4	30	45
	Second	30	0.4	30	50
	Surface	45	1.8	70	120

phonon excitation we note that previous experiments by Theis and Horn[5] have demonstrated that this requires going beyond linear coupling. Work in this direction is in progress.[36] Finally, we wish to note that even if the two-component model used in the decompositions was physically correct, strong couplings exist between the optimum values of the various line shape parameters which prohibit unambiguous determinations of these values.

In order to obtain the best decomposition of the surface peak, the phonon induced structure has to be about twice as intense as the no-phonon line; for the decomposition in Fig. 7 the relative (integrated) intensity is 1.8. It is possible to obtain good decompositions using lower relative intensities than this, however, values below 1 inevitably lead to poor descriptions of the experimental data. Although the relative increase of the core hole–phonon coupling compared to bulk Al is quite large it should be kept in mind that excitation of an average number of phonons of this magnitude or larger is commonly found for metals; the low average number of phonons excited in $2p$ photoemission from bulk Al is quite unique. A stronger coupling to phonons implies a larger probability for multiphonon excitations and thereby larger energy losses. In agreement with this we find that the energy shift between the no-phonon line and the phonon induced structure is slightly larger than found for the bulk peak ($\sim$45 meV compared to $\sim$30 meV) and also the width is larger than what is found for the bulk phonon structure ($\sim$120 meV compared to $\sim$45 meV). Concerning the larger width of the no-phonon line for the surface than for the bulk ($\sim$70 meV compared to $\sim$30 meV in total FWHM), the decompositions do not point to any particular explanation in terms of the increase being attributable to an increase of either the Gaussian or the Lorentzian width. The LEED patterns from the Al(100) surface were of similar high quality as those obtained from the Al(111) surface and it is therefore problematic to simply attribute the increase to a larger disorder broadening for the Al(100) surface. Increasing the crystal field splitting does not result in any significant narrowing of the linewidths of the $2p_{3/2}$ component; a finding which is confirmed by the derivation of a similar increase in width of the $2p_{1/2}$ component for which no crystal field split exists.

Our results in Sec. III D demonstrated that a net force exists on core-excited atoms in the (100) surface layer. The force gives an increase in the phonon coupling relative to the bulk. Couplings to low-energy phonons contribute to the widths of the "no-phonon line" in our two-line decomposition model, and couplings to phonons near the zone boundary to strengths and width of the "replica part." In order to quantify these observations and to obtain a precise phonon broadening line shape, a full *ab initio* study of the lattice dynamics at the surface would be required. The lack of precise knowledge on the phonon broadening prohibits a precise determination of the crystal field split of the $2p_{3/2}$ surface emission from Al(100). This is in contrast to the Al(111) surface emission where a crystal field split very close to zero must be used in order to obtain satisfactory decompositions of the spectra.

V. SUMMARY AND CONCLUSIONS

The surface core-level shifts of Al(111) and Al(100) have been derived from very high resolution core-level photoemission. For the surface layer of Al(111) a shift of -27 ± 3 meV was found. For Al(100) a value of -75 ± 5 meV was found for the first layer whereas the second layer showed a small positive shift of about 20 ± 2 meV. Calculations based on DFT and including final state effects were able to reproduce these experimental shifts. (See Table VIII.)

TABLE VIII. Core-level shifts of the first (SCLS) and second (L2CLS) layer. The experimental geometry is used in the calculations. Energies in meV.

	100		111	
Level	Expt.	Theor.	Expt.	Theor.
SCLS	−75	−71	−27	−14
L2CLS	20	20	0	

Splittings of the core levels induced by the existence of low symmetry crystal fields at the surfaces were investigated in detail. In this respect it was first pointed out that the correct potential to use in such calculations is the one with the core hole present. Inclusion of the core hole was shown to significantly reduce the crystal field splitting of the Al $2p_{3/2}$ level found without such inclusion. Second, it was shown that the treatment has to go beyond the DFT level in order to properly account for the influence of exchange and correlation on the crystal field splitting. When using the full core–valence exchange operator, the contribution from exchange and correlation turns out to be of similar magnitude as the pure Coulomb part but of opposite sign resulting in a total crystal field splitting of close to zero for the Al $2p_{3/2}$ level of surface atoms on Al(111) and Al(100). A very small crystal field split is confirmed experimentally for Al(111) whereas for Al(100) no such conclusion can be made due to insufficient knowledge of the fundamental line shape as discussed below. Inclusion of phonon effects beyond a simple Gaussian broadening was shown to be of vital importance when describing the Al $2p$ spectra. In agreement with previous[31] theoretical calculations, the Al $2p$ bulk line was shown to contain a very narrow no-phonon line and a broad and weak phonon replica. The resulting line shape was found appropriate not only for the bulk emission but also for the second layer peak from Al(100) and the surface emission from Al(111) indicating a bulklike phonon coupling for these layers. For the surface emission from Al(100), however, it was necessary to increase both the linewidth of the no-phonon line as well as the strength of the phonon replica in order to obtain satisfactory decompositions. This was suggested to be caused by a significantly different core hole to phonon coupling for the Al(100) surface layer. Work directed toward obtaining a detailed understanding of the phonon coupling is in progress.[36]

ACKNOWLEDGMENTS

The present work was supported by the Swedish Research Council and by the Danish Natural Science Research Council. The helpfulness of the MAX-lab staff is gratefully acknowledged.

*Deceased Dec. 5, 2002.
[1] W. Eberhardt, G. Kalkoffen, and C. Kunz, Solid State Commun. **32**, 901 (1979).
[2] R. Kammerer *et al.*, Phys. Rev. B **26**, 3491 (1982).
[3] R. Nyholm, J. N. Andersen, J. F. van Acker, and M. Qvarford, Phys. Rev. B **44**, 10987 (1991).
[4] P. S. Bagus, G. Pacchioni, and F. Parmigiani, Phys. Rev. B **43**, 5172 (1991).
[5] W. Theis and K. Horn, Phys. Rev. B **47**, 16060 (1993).
[6] M. Watanabe, T. Kinoshita, A. Kakizaki, and T. Ishii, J. Phys. Soc. Jpn. **65**, 1730 (1996).
[7] T.-C. Chiang and D. E. Eastman, Phys. Rev. B **23**, 6836 (1981).
[8] P. J. Feibelman, Phys. Rev. B **39**, 4866 (1989).
[9] E. Wimmer, M. Weinert, A. J. Freeman, and H. Krakauer, Phys. Rev. B **24**, 2292 (1981).
[10] M. Aldén, H. L. Skriver, and B. Johansson, Phys. Rev. B **50**, 12118 (1994).
[11] R. Nyholm *et al.*, Nucl. Instrum. Methods Phys. Res. A **467–468**, 520 (2001).
[12] P. Hohenberg and W. Kohn, Phys. Rev. **136**, B864 (1964).
[13] W. Kohn and L. J. Sham, Phys. Rev. **140**, A1133 (1965).
[14] O. K. Andersen, Phys. Rev. B **12**, 3060 (1975).
[15] U. von Barth and A. C. Pedroza, Phys. Scr. **32**, 353 (1985).
[16] U. von Barth and R. Car (unpublished).
[17] M. Birgersson, C.-O. Almbladh, M. Borg, and J. N. Andersen, Phys. Rev. B **67**, 045402 (2003).
[18] M. Bockstedte, A. Kely, J. Neugebauer, and M. Scheffler, Comput. Phys. Commun. **107**, 187 (1997).
[19] D. R. Hamann, Phys. Rev. B **40**, 2980 (1989).
[20] P. Blaha *et al.*, *An Augmented Plane Wave plus Local Orbitals Program for Calculating Crystal Properties* (Tech. Universität Wien, Vienna, 2001).
[21] J. P. Perdew, K. Burke, and M. Ernzerhof, Phys. Rev. Lett. **77**, 3865 (1996).
[22] J. H. Petersen, A. Mikkelsen, M. M. Nielsen, and D. L. Adams, Phys. Rev. B **60**, 5963 (1999).
[23] J. Burchhardt, M. M. Nielsen, D. L. Adams, E. Lundgren, and J. N. Andersen, Phys. Rev. B **50**, 4718 (1994).
[24] S. Doniach and M. Šunjić, J. Phys. C **3**, 285 (1970).
[25] G. D. Mahan, Phys. Rev. Lett. **18**, 448 (1967).
[26] G. D. Mahan, Phys. Rev. **163**, 612 (1967).
[27] P. Noziéres and C. de Dominicis, Phys. Rev. **178**, 1097 (1969).
[28] C.-O. Almbladh and L. Hedin, in *Handbook on Synchrotron Radiation*, edited by E. E. Koch (North-Holland, Amsterdam, 1983), Vol. 1b, p. 607.
[29] C.-O. Almbladh, A. L. Morales, and G. Grossmann, Phys. Rev. B **39**, 3489 (1989).
[30] C.-O. Almbladh and P. Minhhagen, Phys. Status Solidi B **85**, 135 (1978).
[31] L. Hedin and A. Rosengren, J. Phys. F: Met. Phys. **7**, 1339 (1977).
[32] M. Birgersson and C.-O. Almbladh, J. Electron Spectrosc. (to be published).
[33] A. R. Edmonds, *Angular Momentum in Quantum Mechanics* (Princeton University Press, Princeton, NJ, 1960).
[34] D. L. Adams and J. N. Andersen (in preparation). The program FitXPS used to fit the XPS spectra with the convolution of a Doniach–Sunjic line form and a Gaussian is available from the authors at http://www.sljus.lu.se/download.html.
[35] J. N. Andersen and C.-O. Almbladh, J. Phys.: Condens. Matter **13**, 11267 (2001).
[36] M. Birgersson *et al.* (unpublished).
[37] L. Hedin, in *X-ray Spectroscopy*, edited by L. V. Azaroff (McGraw-Hill, New York, 1974), p. 226.
[38] The geometrical parameters were determined from plane-wave calculations. The LAPW method gave similar results.